energy&fuels

pubs.acs.org/EF

Article

Highly Robust Zr-MOF Platform Featuring Aromatic-Rich Cores for Efficient Paraffin/Olefin Separation

Published as part of Energy & Fuels special issue "In Honor of Prof. Jingbo Louise Liu - Recipient of 2024 ACS Energy and Fuels Division Mid-Career Award".

Gaurav Verma, Roknuzzaman Roknuzzaman, Kui Tan, Mansi Kapoor, Tony Pham, Sayan Maiti, Joshua Phipps, Sanjay Kumar, Thamraa AlShahrani, and Shengqian Ma*

Cite This: *Energy Fuels* 2025, 39, 11308−11315

Read Online

ACCESS | Metrics & More | Article Recommendations | Supporting Information

ABSTRACT: Paraffin−olefin separations are essential for polymer-grade feedstock production but remain highly energy-intensive via cryogenic distillation, given the similar boiling points and molecular sizes of these hydrocarbons. Metal−organic frameworks (MOFs) provide a promising alternative owing to their high surface areas, tunable porosities, and vast array of functional groups. There is growing interest in reverse-selective MOFs, which favor paraffins via C−H···π interactions between sp^3-hybridized C−H bonds and aromatic regions within the framework. These materials reduce the separation burden on the unadsorbed phase, delivering olefin-enriched streams under comparatively mild conditions. Here, we introduce a zirconium-based MOF (Zr-pbpta) featuring aromatic-rich cores and pyridyl functionalities that achieves notable ethane and propane uptake capacities of 4.55 and 8.50 mmol g^{-1} (1 bar, 298 K), surpassing many benchmark MOFs. It also demonstrates high C_2H_6/C_2H_4 and C_3H_8/C_3H_6 selectivity, driven by strong alkane−framework interactions confirmed via in situ IR measurements. The presence of aromatic moieties and a high density of pyridyl nitrogen sites enabled the high uptake and selectivity observed for the MOF.

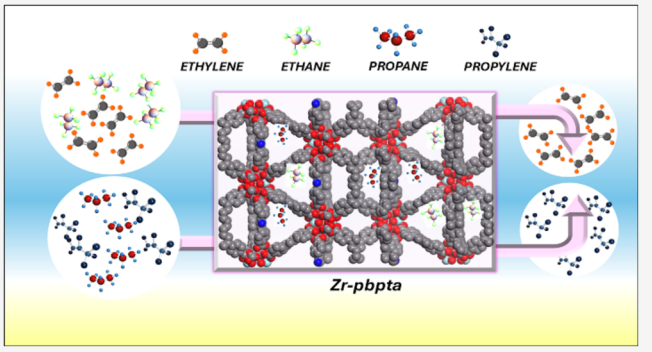

1. INTRODUCTION

The separation of paraffins and olefins is a cornerstone of the petrochemical industry and plays a critical role in producing high-purity feedstocks for a multitude of downstream processes. In particular, the purification of ethane/ethylene (C_2H_6/C_2H_4) and propane/propylene (C_3H_8/C_3H_6) is of immense industrial importance, as ethylene and propylene serve as the primary feedstocks for polymers, solvents, and other fine chemicals. The current annual global production of ethylene and propylene has surpassed 200 million tonnes, reflecting their substantial economic significance.[1] Despite this growing demand, the separation of these hydrocarbon pairs remains challenging due to their remarkably similar physical and chemical properties, as highlighted in Table 1.

Traditionally, paraffin/olefin separations are conducted via cryogenic distillation, a highly energy-intensive process that accounts for substantial energy consumption and environmental impact in petrochemical industries. Remarkably, the separation and purification of C_2H_4 and C_3H_6 are estimated to consume around 0.3% of the global annual energy supply.[3] To address these challenges, significant efforts have been directed toward developing alternative, energy-efficient separation techniques. In response, adsorptive separations using porous materials have gained traction, with metal−organic frameworks (MOFs) emerging as leading candidates due to their ultrahigh porosity, diverse chemistry, molecular-level tunability, selective

Table 1.[2,47] Physical Properties of Ethane, Ethylene, Propane, and Propylene Relevant to Separation

property	ethane (C_2H_6)	ethylene (C_2H_4)	propane (C_3H_8)	propylene (C_3H_6)
molecular weight (g/mol)	30.07	28.05	44.10	42.08
boiling point (°C)	−88.5	−103.7	−42.1	−47.6
kinetic diameter (Å)	4.44	4.16	4.30−5.12	4.68

Received: April 1, 2025
Revised: May 19, 2025
Accepted: May 20, 2025
Published: May 30, 2025

adsorption capabilities, and the potential for reduced operational energy demands.[4]

MOFs are porous crystalline materials composed of metal ions or clusters coordinated by organic linkers, providing well-defined, modifiable pore environments.[5] Unlike conventional adsorbents, MOFs can be methodically designed by modifying organic linkers and inorganic nodes, offering precise control over pore size, shape, and functional groups to allow for discrimination between the different hydrocarbons.[6] Initially, the research largely focused on olefin-selective MOFs utilizing open metal sites or π-complexation with unsaturated hydrocarbons.[7,8] However, reverse-selective MOFs that preferentially adsorb paraffins due to targeted noncovalent interactions are now garnering increasing interest.[9−14] This approach alleviates the regeneration energy typically demanded by strongly bound olefins, yielding an olefin-enrichment stream under comparatively mild conditions.

Paraffin-selective MOFs operate mainly through two fundamental separation mechanisms:[11,15,16] thermodynamic and kinetic. Thermodynamic separations rely on differences in adsorption equilibrium constants, where paraffins exhibit higher affinity toward the MOF due to energetically favorable host−guest interactions. In contrast, kinetic separations exploit differences in diffusion rates through MOF pores, selectively retarding the transport of paraffins or olefins (depending on the MOF structure), thus enabling effective separation. A few other approaches include molecular sieving through carefully tuned pore sizes,[17] or flexible gating mechanisms[18] that can favor the slightly bulkier sp^3-hybridized paraffin molecules.

A crucial aspect contributing to paraffin selectivity is the formation of C−H···π interactions, where aromatic- or electron-rich π-systems within the MOF structure preferentially stabilize the saturated hydrocarbons,[11,19,20] thus enhancing adsorption capacities and selectivities. Notably, ultramicroporous frameworks and certain flexible or functionalized crystalline porous materials (CPM)-derived MOFs have shown promising results for enriching olefins in C_2 and C_3 hydrocarbon mixtures via synergistic pore architectures and tailored C−H···π interactions.[19,21,22] As previously demonstrated by Qian et al.,[23] the presence of an increased number of aromatic rings in the ZJU-120a framework leads to increased ethane uptake capacity and selectivity. A similar effect was observed by our group as well, whereby the presence of aromatic pore surface in Ni-MOF 2 leads to higher C_2H_6 selectivity owing to the presence of unique aromatic pore surfaces.[12] Additionally, donor atoms such as nitrogen or oxygen within functionalized linkers can create specific binding sites that further reinforce paraffin adsorption through induced polarization and dipole interactions.[24,25] Despite these initial advancements, a substantial amount of research is still required to design materials with both enhanced capacity and selectivity.

In this work, we utilized a zirconium-based MOF (Zr-pbpta) endowed with aromatic-rich cores and an abundance of pyridyl donor groups that demonstrated preferential adsorption for ethane and propane over ethylene and propylene, respectively. Built from $[Zr_6(\mu_3\text{-}O)_4(\mu_3\text{−}OH)_4(OH)_4]^{8+}$ clusters and a rectangular linker H_4pbpta (pbpta = 4,4′,4″,4‴-(1,4-phenylenebis(pyridine-4,2,6- triyl))tetrabenzoic acid), the Zr-pbpta showed a high surface area and good stability under various environments. The material displayed high uptake capacities for both ethane and propane that were among some of the top-performing materials, reaching 4.55 mmol g^{-1} and 8.5 mmol g^{-1} at 298 K and 1 bar, respectively. High C_2H_6/C_2H_4 and C_3H_8/C_3H_6 selectivity values were observed, and in situ IR measurements were carried out to elucidate the interaction mechanism that confirmed the presence of strong C−H···π interactions between the alkane and the phenyl rings of the ligand.

2. EXPERIMENTAL SECTION

2.1. Materials and Methods. All of the reagents and solvents were obtained from commercial sources and used without further purification. The ligand H_4pbpta was synthesized according to our previously reported procedure.[26]

Synthesis of Zr-pbpta. Zirconium(IV) chloride (0.233 g, 1.0 mmol) and H_4pbpta (0.214 g, 0.30 mmol) were dissolved in 50 mL of DMF along with an excess of benzoic acid (7.21 g, 59 mmol) as the modulator. This reaction mixture was then heated under reflux for 24 h to yield a yellowish crystalline powder, which was filtered and washed several times with DMF and acetone. The resultant material was solvent-exchanged with ethanol and acetone over 4 days, replacing the solvent 3 times a day. It was then placed under a vacuum oven at 353 K for 6 h to obtain dried Zr-pbpta. FT-IR (cm^{-1}); ν = 3064 (w, br.), 1593 (s), 1548 (m), 1412 (s), 1362 (w), 1180 (w), 1018 (m), 866 (w), 834 (w), 782 (s), 660 (s), 463 (s).

2.2. Instrumentation. Powder X-ray diffraction (PXRD) measurements were performed at room temperature using a Rigaku SmartLab SE diffractometer equipped with Cu Kα radiation (λ = 1.5406 Å) and a secondary monochromator, operating at 40 kV and 50 mA. Data were collected over a 2θ range of 2−30°, with a step size of 0.01° and a scan speed of 4 degrees per minute. Infrared spectra were recorded in the range of 4000−400 cm^{-1} using a Thermo Scientific Nicolet i550 ATR-IR spectrometer with a resolution of 4 cm^{-1}. Scanning electron microscope (SEM) images were collected using a JEOL JSM-IT200 benchtop electron microscope at a 5 kV accelerating voltage, whereby a dried sample of Zr-pbpta was put on carbon tape and analyzed. Single-component gas adsorption (C_2H_4, C_2H_6, C_3H_6, C_3H_8, and N_2) isotherm measurements were conducted using a Micromeritics ASAP 2020Plus surface area and porosity analyzer. Prior to measurements, the as-synthesized samples were activated under dynamic vacuum at 373 K for 12 h on the instrument. The experimental temperatures (77, 273, and 298 K) were controlled by a liquid nitrogen bath, an ice−water bath, and a circulating water bath, respectively.

2.3. *In Situ* Infrared (IR) Spectroscopy Measurements. *In situ* IR measurements were performed on a Nicolet iS50 FTIR spectrometer using a liquid N_2-cooled mercury cadmium telluride (MCT-A) detector. The spectrometer is equipped with a vacuum cell that is placed in the main compartment, with the sample at the focal point of the infrared beam. The samples (~5 mg) were gently pressed onto KBr pellets and placed into a cell that is connected to a vacuum line for evacuation. The samples were activated by overnight evacuation at 100 °C and then cooled back to room temperature for gas adsorption measurement.

3. RESULTS AND DISCUSSION

3.1. Structural Characterization. Zr-pbpta was synthesized according to the previously reported procedures using benzoic acid as the modulator with slight modifications to yield colorless plate-shaped crystals. The Zr-pbpta has been reported previously as MFM-600[27] and Zr-SXU-3[28] in the literature. The structural formula is described as $[Zr_6(\mu_3\text{-}O)_4(\mu_3\text{−}OH)_4(OH)_4(pbpta)_2(H_4pbpta)_{0.7}]$, whereby six Zr(IV) ions form an octahedron capped by μ_3-O/μ_3−OH at each face. Eight edges are bridged by $pbpta^{4-}$ linkers in a bidentate carboxylate mode, while the remaining four equatorial edges each feature a partially occupied H_4pbpta linker (having ~ 35% occupancy) that coordinates in a monodentate fashion via the carboxylic C = O groups (Figure 1a,b). It is interesting to note

https://doi.org/10.1021/acs.energyfuels.5c01684
Energy Fuels 2025, 39, 11308−11315

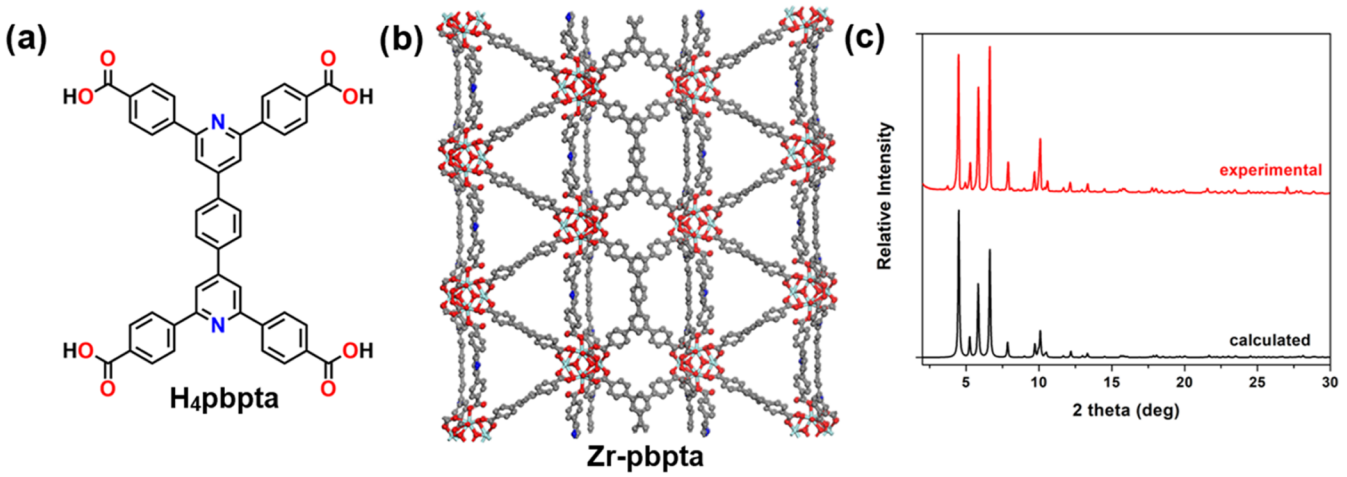

Figure 1. (a) Ligand H_4pbpta, (b) the structural framework of Zr-pbpta, and (c) a comparison of the calculated and experimental PXRD patterns of the as-synthesized material.

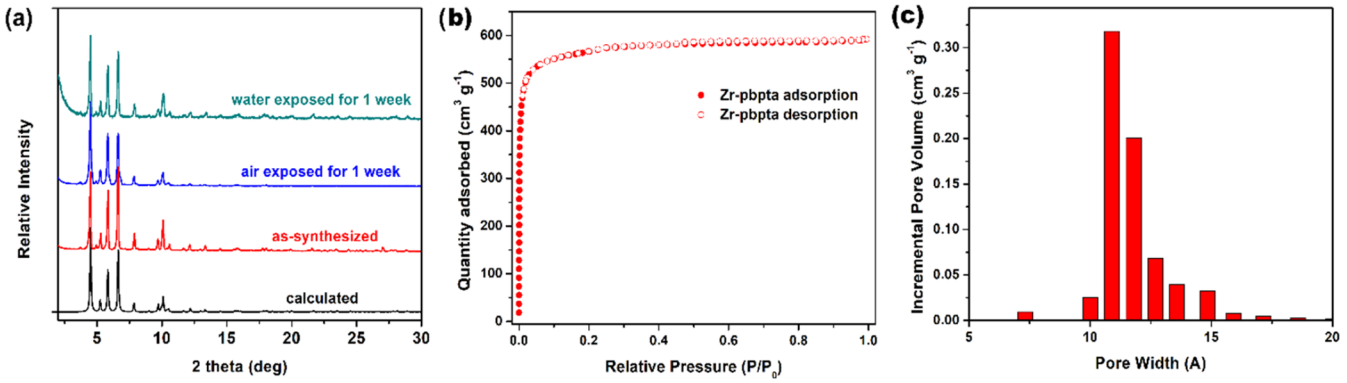

Figure 2. (a) Stability evaluation under various environments, (b) N_2 sorption isotherms at 77 K, and (c) pore size distribution for Zr-pbpta.

that the metal cluster does not contain any open metal site and is decorated with aromatic π-rich cores and abundant pyridyl nitrogen donor atom sites useful for showing interaction with the hydrogen from the alkane.

The bulk phase purity of the material was confirmed by comparing the PXRD of the as-synthesized sample with that of the calculated pattern based on the single-crystal structure. Both showed good agreement with each other, thereby indicating the successful synthesis of Zr-pbpta in high purity (Figure 1b). SEM imaging further established the presence of uniform plate-shaped architectures of sizes <10 μm (Figure S1).

The chemical stability of Zr-pbpta was also examined by exposing it to air and aqueous conditions for a week. As evident from the PXRD patterns shown in Figure 2a, the material shows negligible change in the crystallinity of the framework, thus implying the high robustness of Zr-pbpta under air/aqueous environments. Moreover, the thermogravimetric analysis also shows high thermal stability of the material up to 500 °C (Figure S2), similar to the reported literature.[38]

3.2. Surface Area Measurements. The permanent porosity of Zr-pbpta was verified by N_2 sorption isotherm measurements at 77 K on the sample activated under dynamic vacuum and heat. A type I isotherm with saturated N_2 uptake of 592 $cm^3\ g^{-1}$ was observed (Figure 2b), corresponding to a Brunauer–Emmett–Teller (BET) surface area of 2207 $m^2\ g^{-1}$ and a pore volume of 0.91 $cm^3\ g^{-1}$ that match well with the previously reported values. The pore size distribution evaluated using the nonlinear density functional theory (NLDFT) model displays micropore sizes of 1.0–1.5 nm, as shown in Figure 2c.

3.3. Gas Adsorption Performance. *3.3.1. Ethane/Ethylene Separation.* First, low-pressure C_2H_6 and C_2H_4 single-component adsorption data were collected on the activated samples. As expected, the MOF clearly demonstrated a preferential affinity for paraffin over the olefin, with the uptake capacities reaching 4.55 and 3.27 mmol g^{-1} for C_2H_6 and C_2H_4, respectively, at 298 K and 1 bar (Figure 3a). This ethane uptake capacity is comparable to some benchmark C_2H_6-selective MOFs such as MUF-15[29] (4.69 mmol g^{-1}), Ni(bdc)(ted)$_{0.5}$[30] (5.0 mmol g^{-1}), and JNU-2[31] (4.11 mmol g^{-1}); and much higher than $Fe_2(O)_2$(dobdc)[32] (3.03 mmol g^{-1}), MIL-142A[33] (3.8 mmol g^{-1}), and NUM-7[34] (2.85 mmol g^{-1}). Moreover, the difference in uptake capacity at 1 bar ($\Delta C = C_{C2H6} - C_{C2H4}$) of 1.28 mmol g^{-1} is at par with some of the top-performing materials such as CPM-233[35] (0.93 mmol g^{-1}), TKL-106[36] (1.1 mmol g^{-1}), and Ni(bdc)(ted)$_{0.5}$[30] (1.6 mmol g^{-1}).

At 273 K and 1 bar, the uptake capacities of Zr-pbpta for C_2H_6 and C_2H_4 are 7.26 and 5.41 mmol g^{-1}, respectively (Figure S3). This ethane uptake capacity of Zr-pbpta at 273 K/1 bar is comparable to CPM-233[35] (7.94 mmol g^{-1}) and higher than some of the other top-performing MOFs such as Ni(bdc)(ted)$_{0.5}$[30] (6.93 mmol g^{-1}), PCN-250[37] (6.07 mmol g^{-1}), and ZJU-120a[23] (5.35 mmol g^{-1}).

https://doi.org/10.1021/acs.energyfuels.5c01684
Energy Fuels 2025, 39, 11308–11315

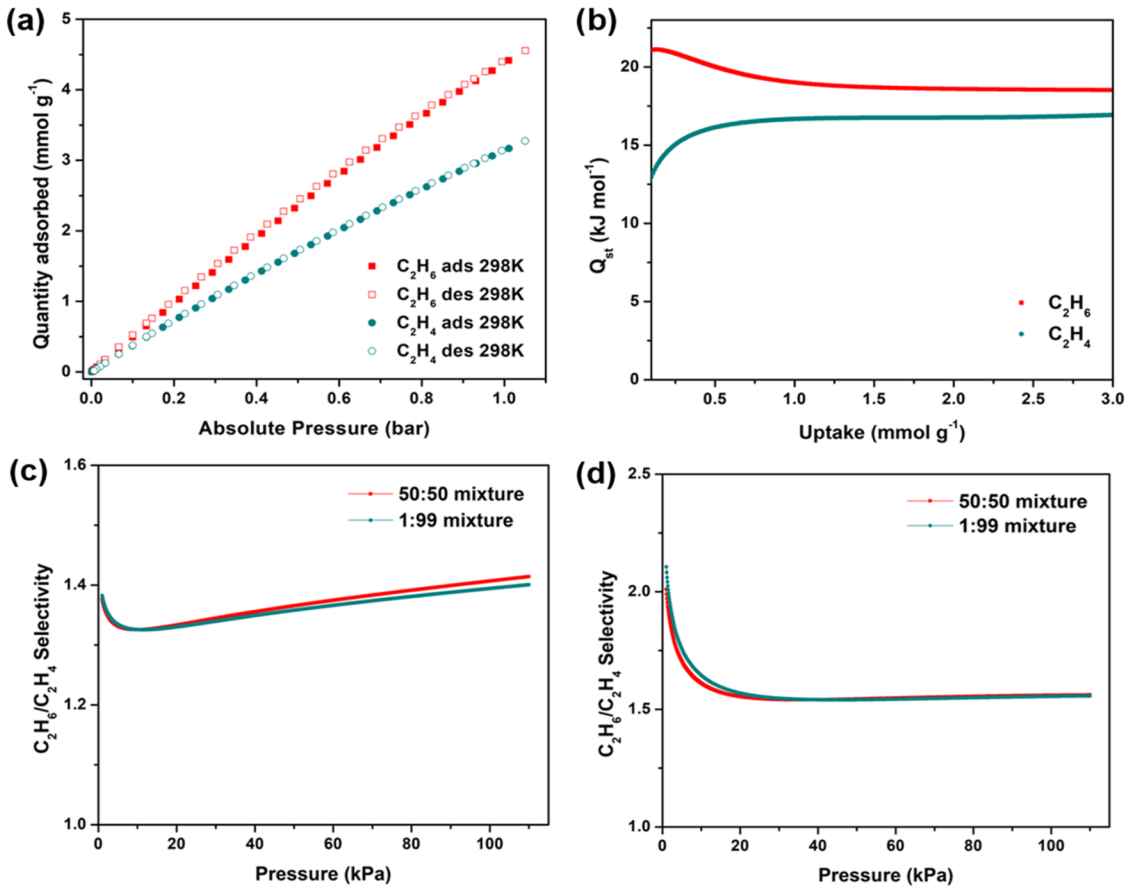

Figure 3. (a) C_2H_6 and C_2H_4 adsorption isotherms of Zr-pbpta at 298 K and 1 bar, and (b) calculated Q_{st} for C_2H_6 and C_2H_4. The calculated IAST selectivity values for 50:50 and 1:99 C_2H_6/C_2H_4 mixtures were obtained at (c) 298 K and (d) 273 K.

The isosteric heat of adsorption (Q_{st}) measurements (Figure 3b) reveal that Zr-pbpta shows a higher Q_{st} value at near-zero loading for C_2H_6 (~21 kJ mol^{-1}) compared to that of C_2H_4 (~13 kJ mol^{-1}), indicating stronger binding affinity and guest-adsorbent interactions with the alkane. Notably, the Q_{st} value for C_2H_6 at near-zero coverage for Zr-pbpta (~21 kJ mol^{-1}) is significantly lower than adsorbents such as $Fe_2(O_2)(dobdc)$[32] (66.8 kJ mol^{-1}), CPM-233[35] (27.3 kJ mol^{-1}), and MUF-15[29] (29.2 kJ mol^{-1}). This implies that lower energy input will be needed for the adsorbent regeneration process, making it more energy-efficient.

To further establish the separation capability of ethane-selective Zr-pbpta, ideal adsorbed solution theory (IAST) was employed to calculate the adsorption selectivities for different C_2H_6/C_2H_4 mixtures. As shown in Figure 3c, high selectivity values up to 1.41 and 1.39 were observed for equimolar (50:50) and excess (1:99) mixtures of C_2H_6/C_2H_4 and 298 K and 1 bar, whereby the selectivity for the equimolar mixture is comparable to some representative MOFs such as MIL-142A[32] (1.5), JNU-2[31] (1.6), and PCN-250[37] (1.52). Similar selectivity values are observed for the excess 1:99 mixture, reaching 1.39 at 1 bar. At 273 K, the selectivity increases slightly to 1.56 and 1.55 for the 50:50 and 1:99 mixtures, respectively (Figure 3d). These results demonstrate the potential of Zr-pbpta as a promising adsorbent for C_2H_6/C_2H_4 separation with a high ethane uptake capacity and selectivity.

3.3.2. Propane/Propylene Separation. Gaining insights from the favorable results obtained for ethane/ethylene separation, we then focused our attention on evaluating the separation capability of Zr-pbpta for propane/propylene separation, another important and highly relevant paraffin/olefin separation process. The C_3H_8 adsorption isotherm collected on activated Zr-pbpta revealed an ultrahigh uptake capacity reaching 8.5 mmol g^{-1} at 298 K and 1 bar (Figure S4). Among the materials reported in the literature for C_3H_8/C_3H_6 separation, only a handful of MOFs such as UiO-67, CPM-736t, and V-bpdc-tph show higher C_3H_8 saturated uptake capacities than Zr-pbpta, with values of 9.38, 10.9, and 11.37 mmol g^{-1}, respectively.[22] Other MOFs such as CPM-734c (8.73 mmol g^{-1}), Zr-BPDC (8.8 mmol g^{-1}), Zr-bipy (8.21 mmol g^{-1}), and FDMOF-2 (6.25 mmol g^{-1}) show similar or lower uptake capacities compared to the Zr-pbpta.[19,20]

As evident in Figure 4a,b, the Zr-pbpta demonstrates higher C_3H_8 uptake compared to C_3H_6 at pressures below 0.45 bar, with a high uptake difference ΔC ($C_{C3H8} - C_{C3H6}$) value of 0.62 mmol g^{-1} at 0.1 bar and 298 K. As the pressures reach 1 bar, a slightly higher uptake of C_3H_6 (9.08 mmol g^{-1}) is observed, while the C_3H_8 uptake reaches 8.5 mmol g^{-1}. This phenomenon is ascribed most likely to the more efficient packing of the smaller C_3H_6 molecules compared to C_3H_8 as the pressures increase, as observed in other high C_3H_8-capacity MOF adsorbents such as CPM-736t, CPM-734t, V-bpdc-tph, and Zr-BPDC.[22,38] At lower pressures, however, stronger host–guest interactions with the larger C_3H_8 molecules lead to greater C_3H_8 uptake. The specific crossover pressure and extent of the uptake difference between C_3H_8 and C_3H_6 depend on both the size and functionality of the linkers used.

https://doi.org/10.1021/acs.energyfuels.5c01684
Energy Fuels 2025, 39, 11308−11315

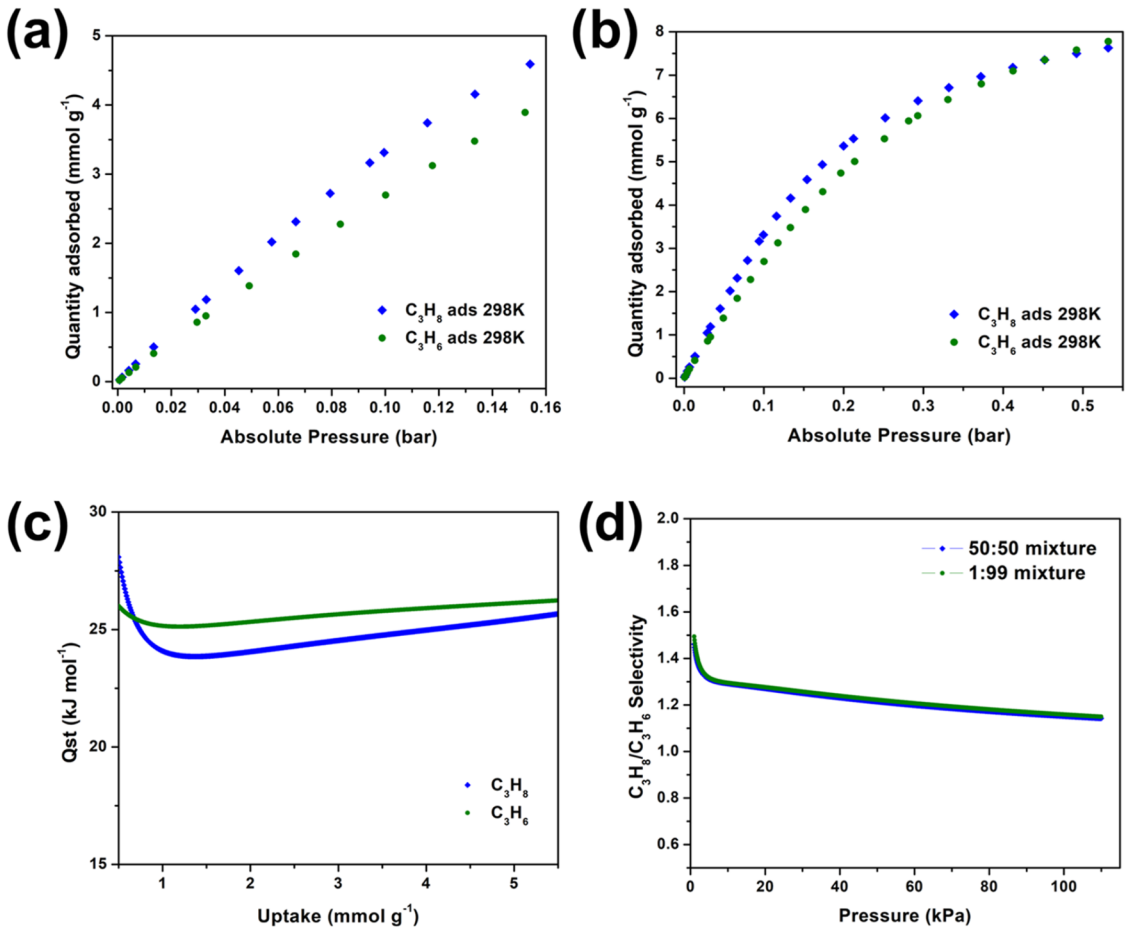

Figure 4. 298 K C_3H_8 and C_3H_6 adsorption isotherms for Zr-pbpta at pressures (a) <0.16 bar and (b) <0.55 bar. Owing to the overlap between adsorption and desorption isotherms, only adsorption isotherms are shown here for the sake of clarity. For full adsorption−desorption isotherms, see the Supporting Information. The Q_{st} values for C_3H_8 and C_3H_6 are shown in (c), while the calculated IAST Selectivity curves for 50:50 and 1:99 C_3H_8/C_3H_6 mixtures at 298 K can be seen from (d).

A similar behavior is observed at 273 K (Figures S5 and S6) whereby the MOF shows a higher uptake capacity for C_3H_8 over C_3H_6 at pressures below 0.3 bar, and as the pressures reach 1 bar, the uptake capacity for C_3H_6 (10.29 mmol g^{-1}) increases slightly in comparison to C_3H_8 (9.53 mmol g^{-1}). The propane uptake capacity of Zr-pbpta at 273 K/1 bar is lower than or comparable to V-bpdc-tph (12.3 mmol g^{-1}), UiO-67 (10.3 mmol g^{-1}), and Zr-bipy (9.77 mmol g^{-1}), but higher than CPM-734t (9.37 mmol g^{-1}) and CPM-734c (9.31 mmol g^{-1}).[19−22]

The isosteric heat of adsorption measurements further confirm the higher binding affinity toward C_3H_8 with the Q_{st} value of 28.1 kJ mol^{-1} at near-zero loading that is higher than the corresponding Q_{st} value of 26 kJ mol^{-1} for C_3H_6 (Figure 4c). Other representative adsorbents such as $Ni(adc)(ted)_{0.5}$ (65.3 kJ mol^{-1}), FDMOF-2 (34.6 kJ mol^{-1}), NUM-7 (40 kJ mol^{-1}), CPM-734c (31.5 kJ mol^{-1}), and CPM-736t (25.2 kJ mol^{-1}) display higher or comparable Q_{st} for C_3H_8.[19,20] Moreover, similarly as for ethane, the heat of adsorption of propane is moderate, thereby facilitating regeneration without the need for a large energy input.

The adsorption selectivity values were further evaluated by using IAST for equimolar (50:50) and excess (1:99) mixtures at 298 K (Figure 4d). The calculated C_3H_8/C_3H_6 selectivity values of Zr-pbpta for a 50:50 mixture at 0.1 and 1 bar are 1.29 and 1.15, respectively. As expected, the selectivity is very high at low pressures (1.46, 0.01 bar) and gradually decreases upon reaching 1 bar. For a 1:99 mixture, similar selectivity values are observed. At 273 K (Figure S7), the selectivity values are much higher for the 50:50 mixture in the low-pressure region at 0.01 bar (2.47) but again decrease upon reaching 0.1 bar (1.34) and 1 bar (1.09). The selectivity values of 1.15 at 1 bar for Zr-pbpta are comparable to those of benchmark MOFs such as V-bpdc-tph (1.24), CPM-736t (1.25), CPM-734c (1.44), Zr-bipy (1.25), and UiO-67 (1.09).[22] Despite moderate selectivity values, these MOFs show superior uptake capacities, thereby rendering them quite attractive for the overall C_3H_8/C_3H_6 separation applications.

3.4. Mechanism Study Using In Situ IR. To gain a deeper understanding of the interaction between Zr-pbpta and adsorbed molecules including $C_2H_6/C_2H_4/C_3H_8/C_3H_6$, we conducted *in situ* infrared (IR) spectroscopy measurements of their loading into the activated sample. Given that the spectra of gas phase are prohibitively high, hindering direct observation of the adsorbed species, we thus evacuated the gas phase by pumping the cell and collected the spectra immediately within ∼5 s of evacuation, i.e., the pressure drops below 500 mTorr that shows negligible gas-phase IR absorption. The spectroscopic results are presented in Figures 5 and S8.

The adsorbed C_2H_6 /C_3H_8 and C_2H_4/C_3H_6 can be readily characterized by their C−H stretching (ν_{as}) and deformation

https://doi.org/10.1021/acs.energyfuels.5c01684
Energy Fuels 2025, 39, 11308−11315

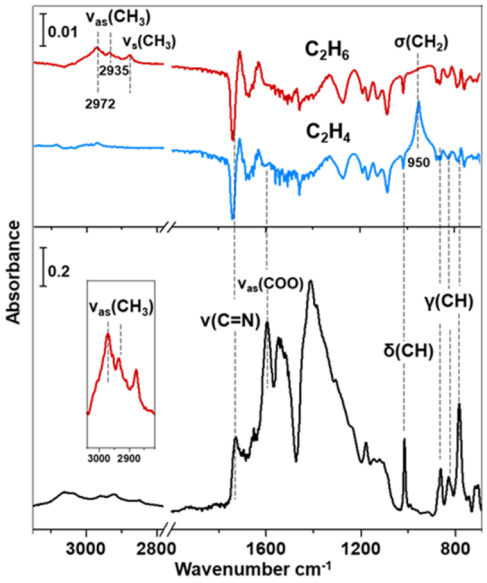

Figure 5. Difference spectra (top) showing the adsorbed C_2H_6 (brown) and C_2H_4 (blue) in Zr-pbpta upon loading of gases at ~300 Torr and 24 °C. Each is referenced to the spectrum of activated Zr-pbpta (bottom). The inset shows $\nu_{as,s}(CH_3)$ bands of adsorbed C_2H_6. Notation and acronym: ν, stretch; σ, deformation; δ, in-plane deformation; γ, out-of-plane deformation; *as*, asymmetric; and *s*, symmetric.

(σ) bands, respectively. Note that these two are the most prominent IR bands of alkanes and alkenes due to their large dipole moment variation.[39−41] Interestingly, C_2H_6 and C_3H_8 show two clearly distinguished $\nu_{as}(-CH_3)$ bands at 2972/2935 and 2958/2932 cm^{-1} in contrast to C_2H_4 and C_3H_6 (see the inset of Figures 5 and S8), which show only one $\sigma(CH_2)$ band at 950 and 912 cm^{-1}. This suggests two types of C_2H_6/C_3H_8 molecules absorbed within Zr-pbpta that give rise to distinct IR absorption features and higher uptake, whereas only one type of C_2H_4/C_3H_6 is present under same condition.[42] We further examined the perturbations occurring to the vibrational bands of the MOF structure upon loading these molecules. Figure 5 shows that the bands associated with the phenyl and pyridine rings of the organic linker are most affected. For instance, CH in-plane (δ) and out-of-plane (γ) deformation modes, which are sensitive to their chemical environment,[43−45] show noticeable decrease in their intensities. The ν(C = N) mode[46] exhibits a slight red shift in position, as typified by the derivative-like feature. In contrast, the metal coordinated carboxylate band ν_{as}(COO) at 1595 cm^{-1} is the least affected, indicating guest molecules interact primarily with the organic linker. The larger perturbations of the linker modes upon loading C_2H_6 imply a stronger interaction of C_2H_6 with the MOF structure.

4. CONCLUSIONS

In the present work, we successfully demonstrated the utilization of Zr-pbpta, having an aromatic-rich core and pyridyl nitrogen functionalities for selective capture of paraffins over olefins. The MOF showed high uptake capacities for ethane and propane at 1 bar and 298 K, reaching 4.55 mmol g^{-1} and 8.50 mmol g^{-1}, respectively. For the propane adsorption, the uptake capacity for Zr-pbpta is much higher than those of many benchmark MOF materials, with a handful of MOFs showing similar or higher values. High C_2H_6/C_2H_4 selectivity values were obtained at 298 K and 1 bar, in accordance with the higher isosteric heat of adsorption (Q_{st}) values observed for ethane compared to ethylene. Similar to the other benchmark propane selective adsorbents, a high C_3H_8/C_3H_6 selectivity was observed at low pressures (<0.45 bar), with slightly higher uptake for propylene at 1 bar and 298 K. As expected, the in situ IR measurements revealed strong interactions of alkanes with the phenyl and pyridyl groups, leading to the high uptake capacities and selectivities observed. Dynamic breakthrough measurements will be carried out in the future to evaluate to determine the selectivity performance.

■ ASSOCIATED CONTENT

Supporting Information

The Supporting Information is available free of charge at https://pubs.acs.org/doi/10.1021/acs.energyfuels.5c01684.

Experimental methods for isosteric heat of adsorption and IAST selectivity (Tables S1 and S2) (Figures S1−S8) (PDF)

■ AUTHOR INFORMATION

Corresponding Author

Shengqian Ma − *Department of Chemistry, University of North Texas, Denton, Texas 76201, United States;* orcid.org/0000-0002-1897-7069; Email: Shengqian.Ma@unt.edu

Authors

Gaurav Verma − *Department of Chemistry, University of North Texas, Denton, Texas 76201, United States*

Roknuzzaman Roknuzzaman − *Department of Chemistry, University of North Texas, Denton, Texas 76201, United States*

Kui Tan − *Department of Chemistry, University of North Texas, Denton, Texas 76201, United States;* orcid.org/0000-0002-5167-7295

Mansi Kapoor − *Department of Chemistry, University of North Texas, Denton, Texas 76201, United States*

Tony Pham − *Department of Chemistry, University of South Florida, Tampa, Florida 33620, United States;* orcid.org/0000-0001-5654-163X

Sayan Maiti − *Department of Chemistry, University of North Texas, Denton, Texas 76201, United States*

Joshua Phipps − *Department of Chemistry, University of North Texas, Denton, Texas 76201, United States*

Sanjay Kumar − *Department of Chemistry, Multani Mal Modi College, Patiala 147001 Punjab, India;* orcid.org/0000-0002-6723-5416

Thamraa AlShahrani − *Department of Physics, College of Science, Princess Nourah bint Abdulrahman University, Riyadh 11564, Saudi Arabia*

Complete contact information is available at: https://pubs.acs.org/10.1021/acs.energyfuels.5c01684

Author Contributions

The manuscript was written through contributions of all authors. All authors have given approval to the final version of the manuscript.

Funding

Robert A. Welch Foundation (B-0027).

Notes

The authors declare no competing financial interest.

■ ACKNOWLEDGMENTS

The authors acknowledge the financial support from the Robert A. Welch Foundation (B-0027) for this work. Partial support from Saudi Water Authority through Energy Innovation Research Chair at Princess Nourah bint Abdulrahman University (T.A.) is also acknowledged.

■ ABBREVIATIONS

CPM, Crystalline Porous Materials; ZJU, Zhejiang University; MFM, Manchester Framework Material; MUF, Massey University Framework; JNU, Jinan University; TKL, Tianjin Key Lab of Metal and Molecule Based Materials; MIL, Matériaux de l'Institut Lavoisier; PCN, Porous Coordination Network; UiO, University of Oslo; bdc, benzenedicarboxylate; ted, triethylenediamine; dobdc, 2,5-dioxido-1,4-benzenedicarboxylate; bpdc, 4,4′-biphenyldicarboxylate; tph, 2,5,8-tri-(4-pyridyl)-1,3,4,6,7,9-hexaazaphenalene; bipy, 2,2′-bipyridine-5,5′-dicarboxylate acid; adc, 9,10-anthracenedicarboxylate

■ REFERENCES

(1) Sholl, D. S.; Lively, R. P. Seven chemical separations to change the world. *Nature* **2016**, *532* (7600), 435−437.
(2) Saha, D.; Toof, B.; Krishna, R.; Orkoulas, G.; Gismondi, P.; Thorpe, R.; Comroe, M. L. Separation of ethane-ethylene and propane-propylene by Ag(I) doped and sulfurized microporous carbon. *Microporpous Mesoporous Mater.* **2020**, *299*, No. 110099.
(3) Jiang, S.; Li, J.; Feng, M.; Chen, R.; Guo, L.; Xu, Q.; Chen, L.; Shen, F.; Zhang, Z.; Yang, Y.; Ren, Q.; Yang, Q.; Bao, Z. Hydrophobic paraffin-selective pillared-layer MOFs for olefin purification. *J. Mater. Chem. A* **2022**, *10* (45), 24127−24136.
(4) Lin, R.-B.; Xiang, S.; Zhou, W.; Chen, B. Microporous Metal-Organic Framework Materials for Gas Separation. *Chem* **2020**, *6* (2), 337−363.
(5) Jiang, C.; Wang, X.; Ouyang, Y.; Lu, K.; Jiang, W.; Xu, H.; Wei, X.; Wang, Z.; Dai, F.; Sun, D. Recent advances in metal−organic frameworks for gas adsorption/separation. *Nanoscale Adv.* **2022**, *4* (9), 2077−2089.
(6) Xie, X.-J.; Zeng, H.; Lu, W.; Li, D. Metal−organic frameworks for hydrocarbon separation: design, progress, and challenges. *J. Mater. Chem. A* **2023**, *11* (38), 20459−20469.
(7) Herm, Z. R.; Bloch, E. D.; Long, J. R. Hydrocarbon Separations in Metal−Organic Frameworks. *Chem. Mater.* **2014**, *26* (1), 323−338.
(8) Bloch, E. D.; Queen, W. L.; Krishna, R.; Zadrozny, J. M.; Brown, C. M.; Long, J. R. Hydrocarbon Separations in a Metal-Organic Framework with Open Iron(II) Coordination Sites. *Science* **2012**, *335* (6076), 1606−1610.
(9) Wu, Y.; Weckhuysen, B. M. Separation and Purification of Hydrocarbons with Porous Materials. *Angew. Chem. Int. Ed* **2021**, *60* (35), 18930−18949.
(10) Ma, L.-L.; Zolotarev, P. N.; Zhou, K.; Zhou, X.; Liu, J.; Miao, J.; Li, S.; Yang, G.-P.; Wang, Y.-Y.; Proserpio, D. M.; Li, J.; Wang, H. Three in one: engineering MOF channels via coordinated water arrays for regulated separation of alkanes and alkenes. *Chem. Sci.* **2024**, *15* (46), 19556−19563.
(11) Saha, D.; Kim, M.-B.; Robinson, A. J.; Babarao, R.; Thallapally, P. K. Elucidating the mechanisms of Paraffin-Olefin separations using nanoporous adsorbents: An overview. *iScience* **2021**, *24* (9), No. 103042.
(12) Ye, Y.; Xie, Y.; Shi, Y.; Gong, L.; Phipps, J.; Al-Enizi, A. M.; Nafady, A.; Chen, B.; Ma, S. A Microporous Metal-Organic Framework with Unique Aromatic Pore Surfaces for High Performance C2H6/C2H4 Separation. *Angew. Chem. Int. Ed.* **2023**, *62* (21), No. e202302564.
(13) Wang, X.; Niu, Z.; Al-Enizi, A. M.; Nafady, A.; Wu, Y.; Aguila, B.; Verma, G.; Wojtas, L.; Chen, Y.-S.; Li, Z.; Ma, S. Pore environment engineering in metal−organic frameworks for efficient ethane/ethylene separation. *J. Mater. Chem. A* **2019**, *7* (22), 13585−13590.
(14) Chen, C.-X.; Wei, Z.-W.; Pham, T.; Lan, P. C.; Zhang, L.; Forrest, K. A.; Chen, S.; Al-Enizi, A. M.; Nafady, A.; Su, C.-Y.; Ma, S. Nanospace Engineering of Metal−Organic Frameworks through Dynamic Spacer Installation of Multifunctionalities for Efficient Separation of Ethane from Ethane/Ethylene Mixtures. *Angew. Chem. Int. Ed.* **2021**, *60* (17), 9680−9685.
(15) Xie, F.; Wang, H.; Li, J. Microporous metal−organic frameworks for the purification of propylene. *J. Mater. Chem.A* **2023**, *11* (24), 12425−12433.
(16) Chitale, S. K.; Jo, D.; Yoon, J. W.; Lee, S.-K.; Cho, K. H.; Lee, U. H. Separation of high-purity propylene through propane-selective CAU-3 isomorphs. *Chem. Phys. Lett.* **2023**, *826*, No. 140687.
(17) Zhang, K.; Pang, J.-J.; Lian, X.; Song, Z.-H.; Yuan, Y.-C.; Huang, H.; Yao, Z.-Q.; Xu, J. A pacs-type metal−organic framework with high adsorption capacity for inverse C2H6/C2H4 separation. *New J. Chem.* **2024**, *48* (23), 10577−10583.
(18) Wang, S.-M.; Shivanna, M.; Zheng, S.-T.; Pham, T.; Forrest, K. A.; Yang, Q.-Y.; Guan, Q.; Space, B.; Kitagawa, S.; Zaworotko, M. J. Ethane/Ethylene Separations in Flexible Diamondoid Coordination Networks via an Ethane-Induced Gate-Opening Mechanism. *J. Am. Chem. Soc.* **2024**, *146* (6), 4153−4161.
(19) Tian, Y.-J.; Deng, C.; Peng, Y.-L.; Zhang, X.; Zhang, Z.; Zaworotko, M. J. State of the art, challenges and prospects in metal−organic frameworks for the separation of binary propylene/propane mixtures. *Coord. Chem. Rev.* **2024**, *506*, No. 215697.
(20) Sadegh, F.; Sadegh, N.; Wongniramaikul, W.; Choodum, A. Recent advances in metal−organic frameworks for C3H6- and C3H8-selective separation of C3H6/C3H8 binary natural gas mixtures: A review. *Fuel* **2024**, *366*, No. 131314.
(21) Xie, X.-J.; Zhou, M.-Y.; Zeng, H.; Lu, W.; Li, D. Pore Engineering in Metal−Organic Frameworks for Enhanced Hydrocarbon Adsorption and Separation. *Acc. Mater. Res.* **2025**, *6* (2), 195−209.
(22) Wang, W.; Chen, Y.; Feng, P.; Bu, X. Tailorable Multi-Modular Pore-Space-Partitioned Vanadium Metal-Organic Frameworks for Gas Separation. *Adv. Mater.* **2024**, *36* (30), No. 2403834.
(23) Pei, J.; Wang, J.-X.; Shao, K.; Yang, Y.; Cui, Y.; Wu, H.; Zhou, W.; Li, B.; Qian, G. Engineering microporous ethane-trapping metal−organic frameworks for boosting ethane/ethylene separation. *J. Mater. Chem. A* **2020**, *8* (7), 3613−3620.
(24) Zhu, Z.; Xiao, J.; Zhang, M.; Wang, Y.; Xin Yao, K.; Yuan, S. Nonpolar microporous Metal-Organic framework decorated with multiple functional sites for efficient Ethane/Ethylene separation. *Sep. Purif. Technol.* **2025**, *354*, No. 128696.
(25) Wang, S.; Zhang, Y.; Tang, Y.; Wen, Y.; Lv, Z.; Liu, S.; Li, X.; Zhou, X. Propane-selective design of zirconium-based MOFs for propylene purification. *Chem. Eng. Sci.* **2020**, *219*, No. 115604.
(26) Verma, G.; Kumar, S.; Pham, T.; Niu, Z.; Wojtas, L.; Perman, J. A.; Chen, Y.-S.; Ma, S. Partially Interpenetrated NbO Topology Metal−Organic Framework Exhibiting Selective Gas Adsorption. *Cryst. Growth Des.* **2017**, *17* (5), 2711−2717.
(27) Carter, J. H.; Han, X.; Moreau, F. Y.; da Silva, I.; Nevin, A.; Godfrey, H. G. W.; Tang, C. C.; Yang, S.; Schröder, M. Exceptional Adsorption and Binding of Sulfur Dioxide in a Robust Zirconium-Based Metal−Organic Framework. *J. Am. Chem. Soc.* **2018**, *140* (46), 15564−15567.
(28) Wang, J.-H.; Li, M.-N.; Yan, S.; Zhang, Y.; Liang, C.-C.; Zhang, X.-M.; Zhang, Y.-B. Modulator-Induced Zr-MOFs Diversification and Investigation of Their Properties in Gas Sorption and Fe3+ Ion Sensing. *Inorg. Chem.* **2020**, *59* (5), 2961−2968.
(29) Qazvini, O. T.; Babarao, R.; Shi, Z.-L.; Zhang, Y.-B.; Telfer, S. G. A Robust Ethane-Trapping Metal−Organic Framework with a High Capacity for Ethylene Purification. *J. Am. Chem. Soc.* **2019**, *141* (12), 5014−5020.
(30) Liang, W.; Xu, F.; Zhou, X.; Xiao, J.; Xia, Q.; Li, Y.; Li, Z. Ethane selective adsorbent Ni(bdc)(ted)0.5 with high uptake and its

significance in adsorption separation of ethane and ethylene. *Chem. Eng. Sci.* **2016**, *148*, 275−281.
(31) Zeng, H.; Xie, X.-J.; Xie, M.; Huang, Y.-L.; Luo, D.; Wang, T.; Zhao, Y.; Lu, W.; Li, D. Cage-Interconnected Metal−Organic Framework with Tailored Apertures for Efficient C2H6/C2H4 Separation under Humid Conditions. *J. Am. Chem. Soc.* **2019**, *141* (51), 20390−20396.
(32) Li, L.; Lin, R.-B.; Krishna, R.; Li, H.; Xiang, S.; Wu, H.; Li, J.; Zhou, W.; Chen, B. Ethane/ethylene separation in a metal-organic framework with iron-peroxo sites. *Science* **2018**, *362* (6413), 443−446.
(33) Chen, Y.; Wu, H.; Lv, D.; Shi, R.; Chen, Y.; Xia, Q.; Li, Z. Highly Adsorptive Separation of Ethane/Ethylene by An Ethane-Selective MOF MIL-142A. *Ind. Eng. Chem. Res.* **2018**, *57* (11), 4063−4069.
(34) Sun, F.-Z.; Yang, S.-Q.; Krishna, R.; Zhang, Y.-H.; Xia, Y.-P.; Hu, T.-L. Microporous Metal−Organic Framework with a Completely Reversed Adsorption Relationship for C2 Hydrocarbons at Room Temperature. *ACS Appl. Mater. Interfaces* **2020**, *12* (5), 6105−6111.
(35) Yang, H.; Wang, Y.; Krishna, R.; Jia, X.; Wang, Y.; Hong, A. N.; Dang, C.; Castillo, H. E.; Bu, X.; Feng, P. Pore-Space-Partition-Enabled Exceptional Ethane Uptake and Ethane-Selective Ethane−Ethylene Separation. *J. Am. Chem. Soc.* **2020**, *142* (5), 2222−2227.
(36) Yu, M.-H.; Fang, H.; Huang, H.-L.; Zhao, M.; Su, Z.-Y.; Nie, H.-X.; Chang, Z.; Hu, T.-L. Tuning the Trade-Off between Ethane/Ethylene Selectivity and Adsorption Capacity within Isoreticular Microporous Metal−Organic Frameworks by Linker Fine-Fluorination. *Small* **2023**, *19* (22), No. 2300821.
(37) Chen, Y.; Qiao, Z.; Wu, H.; Lv, D.; Shi, R.; Xia, Q.; Zhou, J.; Li, Z. An ethane-trapping MOF PCN-250 for highly selective adsorption of ethane over ethylene. *Chem. Eng. Sci.* **2018**, *175*, 110−117.
(38) Yang, S.-Q.; Sun, F.-Z.; Krishna, R.; Zhang, Q.; Zhou, L.; Zhang, Y.-H.; Hu, T.-L. Propane-Trapping Ultramicroporous Metal−Organic Framework in the Low-Pressure Area toward the Purification of Propylene. *ACS Appl. Mater. Interfaces* **2021**, *13* (30), 35990−35996.
(39) Busca, G.; Lorenzelli, V.; Ramis, G.; Sanchez Escribano, V. Chemistry of olefins at metal oxide surfaces: a tool for surface science investigation of oxide catalysts. *Mater. Chem. Phys.* **1991**, *29* (1), 175−189.
(40) Gussoni, M.; Castiglioni, C.; Ramos, M. N.; Rui, M.; Zerbi, G. Infrared intensities: from intensity parameters to an overall understanding of the spectrum. *J. Mol. Struct.* **1990**, *224*, 445−470.
(41) Xie, Y.; Shi, Y.; Cedeño Morales, E. M.; El Karch, A.; Wang, B.; Arman, H.; Tan, K.; Chen, B. Optimal Binding Affinity for Sieving Separation of Propylene from Propane in an Oxyfluoride Anion-Based Metal−Organic Framework. *J. Am. Chem. Soc.* **2023**, *145* (4), 2386−2394.
(42) Kovalev, E. P.; Prikhod'ko, S. A.; Shalygin, A. S.; Martyanov, O. N. Spectral characteristics of ethylene sorbed by silver-containing ionic liquids studied by in situ ATR-FTIR spectroscopy. *Mendeleev Commun.* **2023**, *33* (3), 425−427.
(43) Leclerc, H.; Devic, T.; Devautour-Vinot, S.; Bazin, P.; Audebrand, N.; Férey, G.; Daturi, M.; Vimont, A.; Clet, G. Influence of the Oxidation State of the Metal Center on the Flexibility and Adsorption Properties of a Porous Metal Organic Framework: MIL-47(V). *J. Phys. Chem. C* **2011**, *115* (40), 19828−19840.
(44) Serre, C.; Bourrelly, S.; Vimont, A.; Ramsahye, N. A.; Maurin, G.; Llewellyn, P. L.; Daturi, M.; Filinchuk, Y.; Leynaud, O.; Barnes, P.; Férey, G. An Explanation for the Very Large Breathing Effect of a Metal−Organic Framework during CO2 Adsorption. *Adv. Mater.* **2007**, *19* (17), 2246−2251.
(45) Xie, F.; Chen, L.; Cedeño Morales, E. M.; Ullah, S.; Fu, Y.; Thonhauser, T.; Tan, K.; Bao, Z.; Li, J. Complete separation of benzene-cyclohexene-cyclohexane mixtures via temperature-dependent molecular sieving by a flexible chain-like coordination polymer. *Nat. Commun.* **2024**, *15* (1), No. 2240.
(46) Ibrahim, I.; Yunus, S.; Hashim, A. Relative Performance of Isopropylamine, Pyrrole and Pyridine as Corrosion Inhibitors for Carbon Steels in Saline Water at Mildly Elevated Temperatures. *IJSER* **2013**, *4*, 1−12.
(47) Li, J. R.; Kupplera, R. J.; Zhou, H.-C. Selective gas adsorption and separation in metal−organic frameworks. *Chem. Soc. Rev.* **2009**, *38*, 1477−1504.

https://doi.org/10.1021/acs.energyfuels.5c01684
Energy Fuels 2025, 39, 11308−11315